energies

MDPI

Article

Study on Slagging Characteristics of Co-Combustion of Meager Coal and Spent Cathode Carbon Block

Jigang Zhang, Zijun Liu, Xian Li, Bin Wang, Zhaocai Teng and Kuihua Han *

Shandong Engineering Laboratory for High-Efficiency Energy Conservation and Energy Storage Technology & Equipment, School of Energy and Power Engineering, Shandong University, Jinan 250061, China
* Correspondence: hankh@163.com; Tel.: +86-13589033524; Fax: +86-0531-88392414

Abstract: The harmless disposal of spent cathode carbon blocks (SCCBs) has become an urgent issue in the primary aluminum industry, and the disposal of SCCBs by co-combustion in pulverized coal boilers is expected to be the most effective treatment method. A muffle furnace at 815 °C was used in this study to perform a co-combustion experiment of meager coal and SCCBs. The ash fusion characteristics (AFTs), microscopic morphology, and minerals composition of co-combustion ash were characterized. The interaction mechanism of different mineral components and the change in AFTs and viscosity-temperature characteristics were investigated using FactSage software. Results show that the change in the ash deformation temperature (DT) is correlated linearly with the SCCB addition ratio, whereas other characteristic temperatures exhibit a nonlinear relationship. The contents of SiO_2, Al_2O_3, and Na_2O collectively determine the DT in the ash, and the influence degree from high to low is in the order of SiO_2, Na_2O, and Al_2O_3. The phase diagram of Na_2O–Al_2O_3–SiO_2 is used to accurately predict the changing trend of the melting point of co-combustion ash. The ratio changes between refractory and fusible minerals in the ash, as well as the degree of low-temperature eutectic reaction between sodium- and calcium-containing minerals, are the main factors affecting the melting point of ash. When the blending amount of SCCBs is 5%, mostly complete combustion is achieved, and slagging does not occur easily. The optimal blending ratio of SCCBs is obtained using the co-combustion method from the aspect of AFTs and viscosity-temperature characteristics. This work lays a theoretical foundation for industrial application.

Keywords: meager coal; spent cathode carbon block; co-combustion; ash fusion characteristics; FactSage

check for updates

Citation: Zhang, J.; Liu, Z.; Li, X.; Wang, B.; Teng, Z.; Han, K. Study on Slagging Characteristics of Co-Combustion of Meager Coal and Spent Cathode Carbon Block. *Energies* **2023**, *16*, 736. https://doi.org/10.3390/en16020736

Academic Editor: Adam Smoliński

Received: 12 December 2022
Revised: 2 January 2023
Accepted: 4 January 2023
Published: 8 January 2023

Copyright: © 2023 by the authors. Licensee MDPI, Basel, Switzerland. This article is an open access article distributed under the terms and conditions of the Creative Commons Attribution (CC BY) license (https://creativecommons.org/licenses/by/4.0/).

1. Introduction

Aluminum is an important basic raw material for national economic development. In 2021, the global primary aluminum production capacity was 67.24 million tons, whereas China's production capacity was 38.5 million tons, which constituted approximately 57.26% of the total production capacity. Meanwhile, spent cathode carbon blocks (SCCBs) amounted to approximately 346.5 thousand tons, which were one of the highest hazardous wastes in the aluminum industry [1]. Currently, SCCBs are primarily disposed of using conventional methods such as landfill and stockpiling, which necessitates a significant amount of land resources; more seriously, the harmful substances such as soluble fluoride and cyanide contained in SCCBs cause irreversible pollution to water, air, and soil [2–4]. The treatment methods for SCCBs are primarily categorized into wet and thermal methods. Wet methods include leaching [5–7] and floatation [8] to achieve the recovery of carbon and fluorine. However, none of them has been utilized industrially because of their complex process flow, high energy consumption, and difficulties in secondary pollution control. Thermal methods are combustion methods that use SCCBs which are abundant in carbon and have a relatively high calorific value as an alternative fuel or a reductant, mainly include high temperature roasting [9], collaborative disposal [10], and reduction [11], which

are considered as the most promising treatment methods for SCCBs. However, this disposal is not adopted broadly owing to high treatment costs and uneven regional distributions of reuse enterprises. This issue has become a bottleneck in the development of the aluminum industry. As a simple and effective method, co-combustion is worthy of further study.

Combustion is the most typical method to dispose of hazardous waste, and it is an effective method for utilizing resources [12,13]. Although scholars have conducted a lot of research on the co-combustion of carbonaceous materials [14,15] as a hazardous waste with complex composition and characteristics, the co-combustion of SCCB with coal is still relatively novel and worth studying. Zhang et al. investigated the combustion characteristics and kinetic behavior of co-combustion coal with SCCBs at different blending ratios and proposed the co-disposal of SCCBs using pulverized coal boilers [16]; however, they did not study the ash fusibility, corrosion during the co-combustion of coal and SCCBs. SCCBs are abundant in elements such as Na and F. Their direct combustion releases corrosive gases such as HF and SiF_4, as well as generates low-melting-point sodium salt, thereby causing problems such as equipment corrosion and easy slagging [17,18]. Considering the safety and stability of long-term boiler operation, an in-depth study regarding the ash accumulation, slagging, and corrosion of SCCB co-combustion with coal is necessitated; so far, only a few relevant studies have been reported.

The AFTs are one of the most important parameters to determine the tendency of the fuel to slag and accumulate ash [19] and are usually characterized by the DT, softening temperature (ST), hemispheric temperature (HT), and flow temperature (FT). Previous studies have concluded that AFTs are closely related to the composition of ash and mineral, as well as mineral changes during melting [18,20,21]. However, the ash melting characteristics of blended coals are non-linear and cannot be discerned entirely by the slagging of the component single coals [22–24]. Therefore, it is particularly important to study the melting characteristics of co-combustion ash of SCCBs and coal. In this study, two samples of meager coal and SCCB were used to perform ash melting experiments based on different blending ratios. The slagging index and characteristic temperature were calculated, and the relationship between the ash melting point and ash content was investigated. X-ray fluorescence (XRF), X-ray diffractometer (XRD), scanning electron microscopy (SEM), and other methods were used to analyze the AFTs of the mixed samples. The FactSage7.0 thermodynamic software was used to establish a co-combustion ash system of Na_2O–Al_2O_3–SiO_2–CaO–Fe_2O_3 and investigate the mineral composition changes of different co-combustion ash with respect to temperature. The variable temperature phase diagram of Na_2O–Al_2O_3–SiO_2 and the flow temperature obtained from the experiment were compared and analyzed. Subsequently, the viscosity of the ash was calculated. The effects of additives on mineral composition and viscosity-temperature characteristics were also considered. This study reveals the mechanism of ash agglomeration of SCCBs and meager coal during the co-combustion process, which provides an important reference for the large-scale disposal of SCCBs using the co-combustion method in coal-fired boilers.

2. Experiment

2.1. Preparation of Ash Sample

The meager coal was purchased from Taiyuan, Shanxi Province, China. The SCCBs were produced from an aluminum electrolytic cell used by Shandong Weiqiao Aluminum and Electricity Co., Ltd. for 5 years. The meager coal and SCCBs were pulverized and dried and then grounded evenly using a grinding pestle. After sieving, powder measuring less than 0.125 mm was obtained. Subsequently, meager coal and SCCBs of different qualities were placed in the experimental mixer and mixed thoroughly for 30 min, after which fully mixed samples were obtained and stored in a glass desiccator. The mass of each sample was 10 g. The mass proportions of the SCCBs in the mixture were 0%, 5%, 10%, 15%, 20%, 25%, 30%, 35%, 40%, 45%, 50%, and 100%. The prepared sample was named SCCB-X (where X represents the proportion of SCCBs, and 100-X represents the proportion of meager coal).

First, 2 ± 0.01 g of the sample was obtained from the dryer and placed in an ash pan; subsequently, it was put into the muffle furnace. The temperature of the furnace was increased to 500 °C at a rate of 5 °C/min and maintained for 30 min. Subsequently, it was increased to 815 °C at a rate of 5 °C/min and then burned for 1 h. Finally, the ash pan was removed after it was cooled down to room temperature and then placed in a desiccator on a heat-resistant plate to obtain ash samples of different mixing ratios.

2.2. Determination of Ash Melting Point

The ash samples were formed into ash cones with a base length of 7 mm and a height of 20 mm, and the ash melting points of the 12 groups of ash samples were measured under a weak oxidizing atmosphere using a ZDHR-3 ash melting point tester. Subsequently, the characteristic melting temperature of the ash was measured according to the Chinese National Standard GB/T219-2008.

2.3. Characterization of Ash

A PANalytical Axios sequential wavelength dispersive X-ray fluorescence spectrometer (XRF) was used to determine the composition and content of each element in the ash sample, and an X-ray diffraction analyzer (XRD, Rigaku Corporation, Tokyo, Japan) was used to detect minerals contained in the meager coal, SCCB, and ash, based on a scanning angle of 5°–90°, scanning speed of 5°/min, and step size of 0.02°. Furthermore, scanning electron microscopy (SEM, JEOL, Tokyo, Japan) was performed to observe the micromorphology of the ash samples.

2.4. Analysis Method

In general, the chemical composition of ash can be categorized into two groups: acidic components with high melting points ($SiO_2 + Al_2O_3 + TiO_2$) and alkaline components that serve as fluxes to lower the melting points ($Fe_2O_3 + CaO + MgO + Na_2O + K_2O$) [25]. The effective prediction of the slagging characteristics of coal combustion has aroused the interest of domestic and foreign scholars, and many methods have been proposed to predict slagging [26–28]. Table 1 shows the indices used in this study for the qualitative analysis of the slagging characteristics [29,30].

Table 1. Summary of some existing coal slagging indices.

Index	Index Expression	Slagging Potential			
		Low	Medium	High	Severe
$R_{B/A}$	$R_{B/A} = \frac{(Fe_2O_3+CaO+MgO+Na_2O+K_2O)}{(SiO_2+Al_2O_3+TiO_2)}$	<0.206	0.206–0.4	>0.4	—
S_R	$S_R = 100 \times \frac{SiO_2}{(SiO_2+Fe_2O_3+CaO+MgO)}$	>78.8	66.1–78.8	<66.1	—
F_u	$F_u = \frac{(Fe_2O_3+CaO+MgO+K_2O+Na_2O)}{(SiO_2+Al_2O_3+TiO_2)} \times (Na_2O + K_2O)$	<0.6	—	0.6-40	>40
F_s	$F_s = \frac{4DT+HT}{5}$	>1343 °C	1232–1343 °C	1149–1232 °C	<1149 °C

Note: Alkali-acid ratio ($R_{B/A}$), slag viscosity index (S_R), fouling index (F_u), and slagging index (F_s).

2.5. Thermodynamic Calculation

Based on the chemical composition of ash, the Equilib module in the FactSage7.0 thermodynamic software was used, and the FToxid database was selected to establish the Na_2O–Al_2O_3–SiO_2–CaO–Fe_2O_3 system for the co-combustion ash. Using temperature as a variable, the changes in the mineral composition of different co-fired ash during the temperature increase from 900 °C to 1600 °C were investigated, and the temperature interval was 100 °C. Furthermore, In addition, the ternary phase diagrams of a Na_2O-Al_2O_3-SiO_2 system with constant CaO content and a CaO-Al_2O_3-SiO_2 system with constant Na_2O content are drawn by the phase diagram module. Finally, the viscosity-temperature characteristics of different co-combustion ashes were calculated using the viscosity module.

3. Results and Discussion

3.1. Ash Composition Analysis

The composition and content of each element in the SCCB-X ash are listed in Table 2. As shown in Table 2, the SCCB ash is abundant in Na_2O (32.80%), Al_2O_3 (32.31%), and SiO_2 (23.44%), and the meager coal ash is abundant in Al_2O_3 (32.91%) and SiO_2 (49.56%) but low in Na_2O (0.62%), which is similar to the composition of other samples reported in the literature [31]. As the SCCB blending amount increased, the content of Na_2O increased, and the content of SiO_2 decreased gradually. However, the mass fraction remained beyond 38.92%. When the temperature is higher than 900 °C, SiO_2 can easily react with the alkaline components (Na_2O and CaO) to produce silicate containing sodium and calcium (Na_2SiO_3 and $CaSiO_3$). Furthermore, it can form a low-temperature eutectic of sodium- and calcium-containing minerals (Na_2CaSiO_4) [32], thereby reducing the AFTs. Generally, the acidic components have the function of increasing FT, while the basic components have the function of reducing FT [33–36]. However, when the SiO_2 content is extremely high, the monomeric SiO_2 with a high melting point (1600 °C) causes an increase in the ash melting point, which reflects the duality of the effect of SiO_2 on AFTs. The volatilization and release of sodium at high temperatures may reduce the effect of sodium on the melting temperature [37].

Table 2. Analysis of ash composition of meager coal, SCCB, and their mixed samples.

Sample	Na_2O	MgO	Al_2O_3	SiO_2	P_2O_5	SO_3	K_2O	CaO	TiO_2	Fe_2O_3	Others
SCCB-0	0.62	0.83	32.91	49.56	0.19	1.03	0.98	3.17	1.03	6.28	3.40
SCCB-5	1.86	0.39	34.87	45.45	0.94	3.94	1.24	2.62	1.45	5.76	1.48
SCCB-10	4.31	0.38	34.39	42.94	0.88	5.12	1.16	3.52	1.33	5.43	0.54
SCCB-15	7.31	0.38	33.99	39.67	0.37	6.71	1.09	3.66	1.24	5.18	0.40
SCCB-20	7.70	0.44	33.83	38.92	0.93	5.78	1.47	3.84	1.29	5.27	0.53
SCCB-25	11.43	0.41	33.83	34.82	0.62	6.92	1.18	4.07	1.12	5.04	0.56
SCCB-30	13.36	0.36	34.04	32.83	0.55	7.16	0.93	4.23	1.11	4.88	0.55
SCCB-35	14.04	0.80	33.81	32.56	0.23	8.19	0.90	3.79	0.96	4.39	0.33
SCCB-40	16.87	0.27	34.77	31.30	0.67	4.57	1.71	4.02	0.95	4.46	0.41
SCCB-45	17.59	0.87	34.74	28.28	0.23	7.90	1.17	3.99	0.84	4.07	0.32
SCCB-50	17.95	0.87	34.72	27.38	0.11	8.77	0.89	4.10	0.80	4.07	0.34
SCCB-100	32.80	0.83	32.31	23.44	0.06	0.15	0.70	4.09	0.47	4.39	0.76

As the SCCB blending amount increased, the Al_2O_3 content increased slightly. The Al_2O_3 content of the meager coal ash was the lowest at 32.91%, which was relatively high. It served as a skeleton in the ash melt and hindered the deformation of the melt, thereby reducing slagging. Simultaneously, the Fe_2O_3 content decreased gradually. The study by Zhao et al. [38] showed that in an oxidizing atmosphere, Fe_2O_3 with a high melting point barely participated in the reaction; however, when the content was low, it dissolved rapidly in the solution, causing it to rapidly reach the flow temperature. Fe_2O_3 is an alkaline oxide with low ionic potential energy, which can destroy the polymers in ash melt and play the role of solvent. It was reported that when the content of Fe_2O_3 was less than 20%, the softening temperature decreased by about 12.7 °C with every 1% increase in Fe_2O_3 content [39]. In addition, with the increase in the SCCB blending content, the content of CaO did not change significantly (2.62–4.23 wt.%), and the contents of MgO, K_2O, and TiO_2 were low (total of 2.0–3.08 wt.%). Therefore, they did not significantly affect the melting temperature of the ash.

3.2. Analysis of Ash Melting Characteristics

3.2.1. Characteristic Index Analysis

The results of the slagging index calculations for the combustion ash of the meager coal, SCCB, and their mixed samples are shown in Table 3. Compared with the meager coal ash, the SCCB ash is abundant in Na, low in Si, and has a similar Al content. The $R_{B/A}$, S_R,

and F_u values of the SCCB ash were 0.598, 71.57, and 13.036, respectively, indicating that the slagging of the combustion process was relatively severe. This is due to the high Na content of the SCCB. The $R_{B/A}$, S_R, and F_u of the meager coal ash were 0.142, 82.82, and 0.088, respectively. These values reflect the high Si content, which serves as a skeleton in the ash and exists primarily in the form of silicate crystals with a high melting point and less slagging.

Table 3. Slagging index of mixed sample ash.

Sample	$R_{B/A}$	S_R	F_u	F_s
SCCB-0	0.142	82.82	0.088	1402
SCCB-5	0.145	83.83	0.270	1383
SCCB-10	0.188	82.15	0.810	1364.6
SCCB-15	0.235	81.14	1.718	1356.8
SCCB-20	0.253	80.30	1.948	1334.8
SCCB-25	0.317	78.53	3.623	1309
SCCB-30	0.350	77.61	4.676	1297.6
SCCB-35	0.355	78.38	4.984	1281.6
SCCB-40	0.408	78.15	6.883	1281
SCCB-45	0.434	76.00	7.634	1255.4
SCCB-50	0.443	75.18	7.952	1245.4

As the content of SCCBs increased, $R_{B/A}$ and F_u increased, whereas S_R decreased. When the blending amount of SCCBs reached 10%, the F_u value of ash was 0.810; when it reached 15%, the $R_{B/A}$ value of ash was 0.235; meanwhile, when it exceeded 20%, the S_R value of ash was 78.53, which may be regarded as medium caking based on the corresponding standard. This is because when mixed with a small number of SCCBs, which contains less Na, the high content of Al_2O_3 easily reacts with SiO_2 to generate high-melting-point mullite ($3Al_2O_3+2SiO_2 \overset{1100°C}{\rightarrow} 3Al_2O_3 \cdot 2SiO_2$); at a high temperature of 1600 °C, volatilization is not decomposed. When the Na content in the ash is sufficiently high, a eutectic phase occurs between Al_2O_3 and SiO_2, which resulted in the deposition of low-melting-point sodium feldspar ($Na_2O + Al_2O_3+6SiO_2 \overset{970°C}{\rightarrow} 2NaAlSi_3O_8$) on the walls of the heat exchanger tubes and intensified the accumulation of ash slagging [40]. It was shown that at high temperatures, the Si–Al in the ash trapped sodium and retained it in the ash slag [41,42]. Therefore, Na was the main cause of slagging affecting the co-combustion of SCCBs with coal, and similar conclusions have been reported in studies pertaining to biomass co-combustion with coal [43]. Based on an analysis of the slagging characteristics, the blending amount of SCCBs should not exceed 10%.

3.2.2. AFT Analysis

The AFT of ash can reflect its dynamic deposition characteristics in a boiler [44]. Figure 1 and Table S1 show the characteristic temperatures of the co-combustion ash of meager coal and SCCBs at different blending ratios. The DT of meager coal ash was the lowest (1384 °C), whereas the DT of SCCB ash was the highest (1444 °C); as the amount of SCCB blending increased, its deformation temperature decreased gradually. The ST exhibited a change law similar to the DT. The FT of mixed combustion ash exceeded 1400 °C, and it did not satisfy the requirements of liquid discharge [45]. However, pulverized coal furnaces generally use solid slag discharge, and the boiler heating surface does not form severe coking.

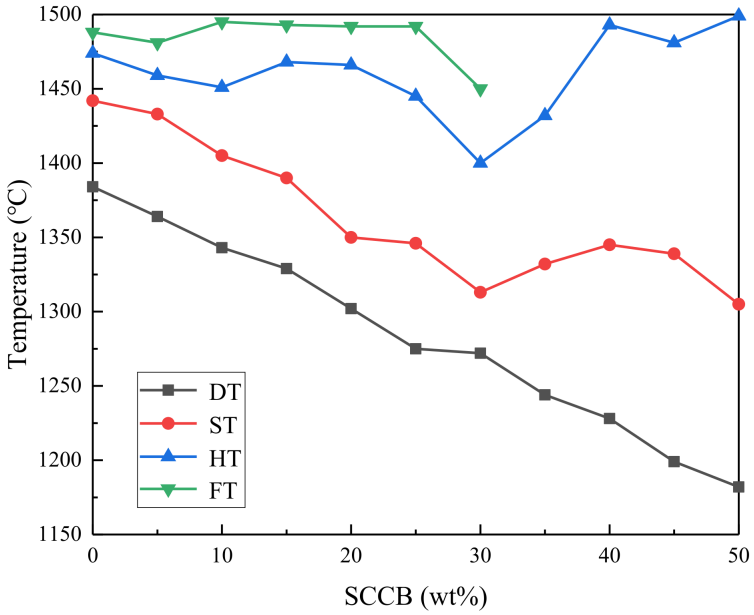


Figure 1. Ash fusion temperature curve of co-combustion ash of SCCB-X.

3.2.3. Correlation Analysis between DT and Characteristic Index

Figure 2 shows the relationship between DT and the characteristic index of co-combustion ash of SCCB-X. As shown in Figure 2, with the decrease of DT, the alkali-acid ratio ($R_{B/A}$) and fouling index (F_u) increase, while the slag viscosity index (S_R) and slagging index (F_s) decrease, indicating that DT and characteristic index are linearly correlated. This is due to the increase of alkali metal content, easy to produce low-melting-point of minerals, resulting in the decrease of ash melting point and the increase of slagging tendency.

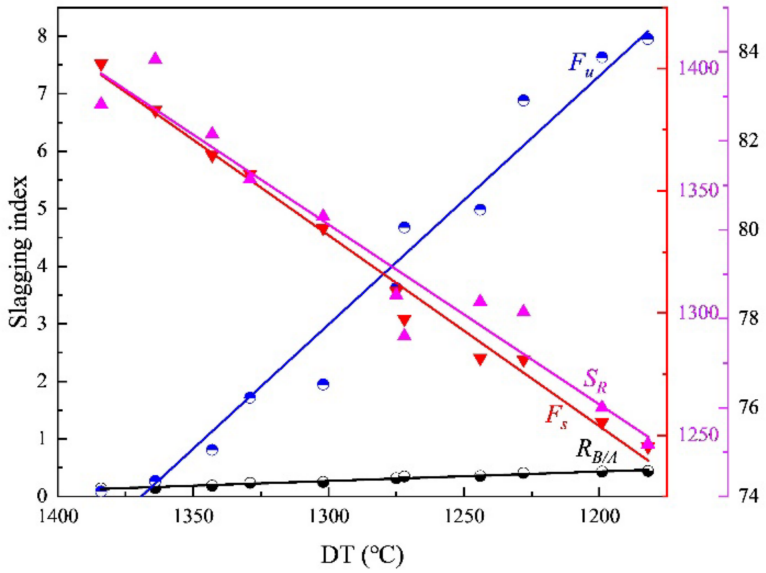


Figure 2. Relation between DT and the characteristic index of co-combustion ash.

3.3. Relationship between Ash Melting Point and Ash Content

3.3.1. Single Oxide Evaluation

A DT with a larger temperature range was selected as the research object to investigate the relationship between the ash melting temperature and the ash composition. Figure 3 shows the relationship between the single ash content and DT. Compared with meager coal, the SCCB exhibited a higher degree of carbonization, a more complex composition

in ash, and a higher DT. Three typical oxides (Na_2O, Al_2O_3, and SiO_2) of the ash were selected. It was observed that the Al_2O_3 variation range of SCCB-X was only 5.46%, which was much smaller than 21.18% for Na_2O and 26.12% for SiO_2. Regarding the effect of a single component in the ash on the DT, the regularity of the effect of the Al_2O_3 content on the DT was insignificant and hence will not be explained herein. The change in the Na_2O and SiO_2 contents significantly affected the DT. The linear regression coefficient R^2 exceeded 0.95, which implied a close reflection of the real situation. The slope of the fitted line shows that the content of Na_2O was positively correlated with the DT, whereas SiO_2 was negatively correlated with the DT. Therefore, for the single oxide in the ash of SCCB-X, Na_2O increased the DT, whereas SiO_2 imposed the opposite effect. The absolute value of the slope of the fitted line segment indicates the degree of influence, where the higher the absolute value, the greater the effect of the change in the independent variable on the dependent variable. The oxide content was the independent variable, whereas the DT was the dependent variable. The degree of influence of the three oxides was in the following order: $SiO_2 > Na_2O > Al_2O_3$.

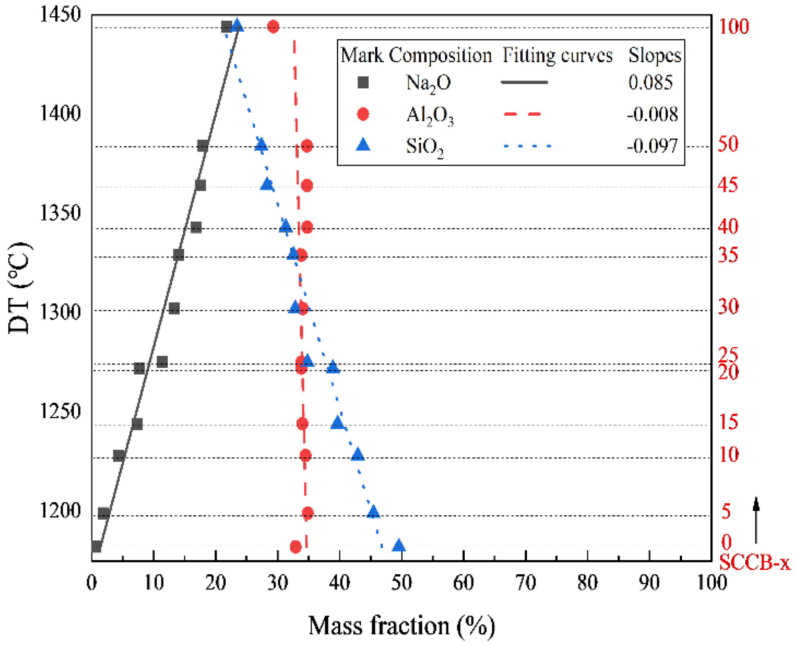


Figure 3. Relationship between single ash content and DT.

3.3.2. Phase Diagram Analysis

As shown in Table 1, the contents of Al_2O_3, CaO, Na_2O, and SiO_2 in the SCCB-X co-combustion ash exceeded 84%, and the content of CaO did not change significantly. Therefore, this system can be simplified to a Na_2O–Al_2O_3–SiO_2–CaO system with a fixed CaO mass fraction (4.0%). Meanwhile, a CaO-Al_2O_3-SiO_2-Na_2O system with a fixed mass fraction of Na_2O (2.0%) was constructed to investigate the effect of adding CaO on the melting characteristics of ash. The simulation results obtained using FactSage are presented in Figures 4 and 5.

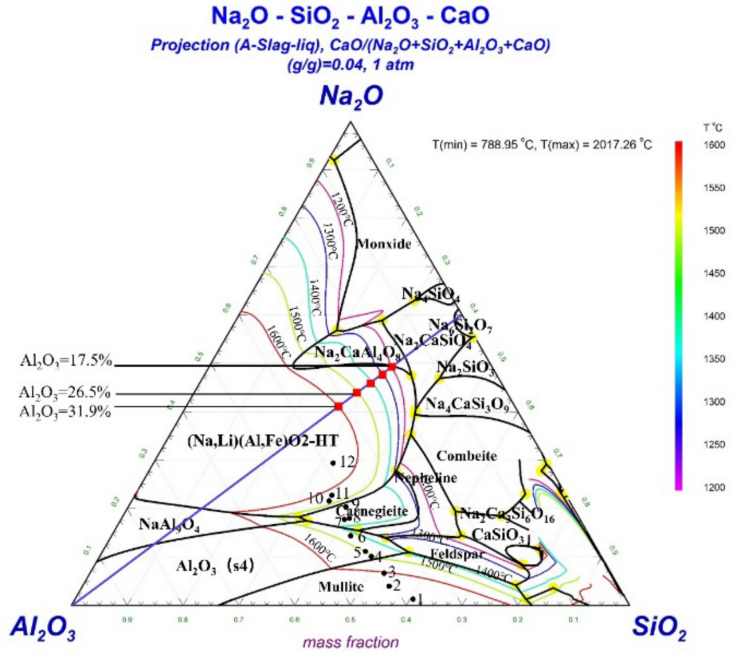


Figure 4. Ternary phase diagram of a Na_2O–Al_2O_3–SiO_2–CaO system.

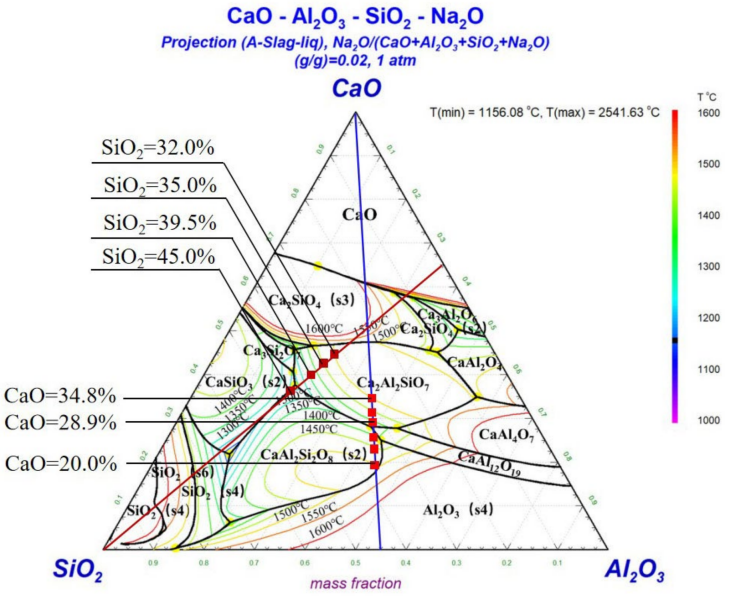


Figure 5. Ternary phase diagram of a Na_2O-Al_2O_3-SiO_2-CaO system.

The phase diagram was used to convert the components of each ash sample, and dots were used in the figure to represent the location of the SCCB-X ash sample. Points 1 and 2 represent the ash samples of SCCB-0 and SCCB-5, respectively. The melting temperature can be determined at different locations. The flow temperature at Point 6 was the lowest, i.e., approximately 1420 °C, and the experimental value was 1492 °C. The flow temperatures at Points 1, 2, and 12 were some of the highest, i.e., exceeding 1600 °C. However, owing to the limitations of the experimental conditions, the experimental value could not be measured. It is noteworthy that the experimental results can be reflected in the phase diagram. Similar conclusions have been obtained from existing studies [32].

Figure 4 shows the phase change function of the Al_2O_3 content when the mass ratio of Na_2O/SiO_2 was 3/2. The first point in the upper left corner reflects the Al_2O_3 content of 17.5%, and it is located in the phase field of $Na_2CaAl_4O_8$; additionally, the liquidus tem-

perature at this time is 1200 °C. As the Al_2O_3 content increased, the chemical composition of the mixed ash shifted toward the feldspar phase field, and the liquidus temperature increased gradually. When the Al_2O_3 content reached 31.9%, the liquidus temperature reached 1600 °C. When the Al_2O_3 content continued to increase, the liquidus temperature of the sample continued to increase. The trend shown in the phase diagram was similar to the flow temperature result of ash melting.

Figure 5 shows the ternary phase diagram of variable temperature in the Al_2O_3-SiO_2-CaO system when the mass fraction of Na_2O is 2.0%. The red line shows the phase change function of SiO_2 content when the mass ratio of CaO/Al_2O_3 is 13/7. The first point in the upper left corner indicates that when the content of SiO_2 is 32.0%, it is located in the phase field of $Ca_2Al_2SiO_7$, and the liquidus temperature at this time is 1500 °C. With the increase of SiO_2 content, the chemical composition of the mixed ash moves towards the $CaAl_2Si_2O_8$ or $CaSiO_3$ phase field, and the liquidus temperature decreases gradually. When the content of SiO_2 reaches 39.5%, the liquidus temperature drops to 1350 °C. This reflects the duality of the influence of SiO_2 on ash melting characteristics [37].

The blue line shows the phase change function of CaO content when the mass ratio of SiO_2/Al_2O_3 is 9/11. The first point in the lower middle corner indicates that when the content of CaO is 20.0%, it is located in the phase field of $CaAl_2Si_2O_8$, and the liquidus temperature is 1500 °C. With the increase of CaO content, the chemical composition of the mixed ash moves towards the $Ca_2Al_2SiO_7$ phase field, and the liquidus temperature firstly decreases and then increases. When the CaO content reaches 28.9%, the liquidus temperature drops to 1450 °C, which may be due to the low temperature eumelt formed by CaO and the high melting point minerals in the system, which reduces the melting temperature of ash. When the CaO content further increases to 34.8%, the liquidus temperature rises to 1500 °C, which is because the excessive CaO monomer in the ash raises the ash melting temperature.

3.4. Mineral Composition during Ash Melting

Changes in the mineral type, content, and liquid phase line can be used to predict changes in the ash melting temperature. It has been demonstrated that FactSage is an important tool for explaining the variation in ash flow properties and can accurately predict the mineral transformation process of ash [46,47]. As shown in Table 2, the contents of MgO, K_2O, and TiO_2 in the co-combustion ash were extremely low and varied only slightly; therefore, its effect on the ash melting characteristics was not considered in this study. The FactSage 7.0 thermodynamic software was used to calculate the mineral composition of combustion ash at different blending amounts.

Figure 6 shows that the meager coal ash has a liquid phase at 1200 °C. As the temperature increased, the liquid phase content increased significantly and then transformed completely into the liquid phase at 1534 °C. This explains the higher melting temperature of the meager coal ash. The main refractory components in the SCCB-X ash were composite oxides ($Al_2O_3 \cdot Fe_2O_3$), anorthite ($CaAl_2Si_2O_8$), albite ($NaAlSi_3O_8$), and quartz (SiO_2). As the SCCB content increased from 0% to 20%, the types of insoluble matter in the ash decreased. The liquidus temperatures were 1534 °C, 1540 °C, 1496 °C, 1450 °C, and 1432 °C for the abovementioned materials, respectively, showing a decreasing trend. This is because the increase in Na_2O promoted the production of sodium feldspar, which has a low melting point (1100 °C) and an excellent fluxing effect on fusible minerals such as quartz [48,49], resulting in a further decrease in the melting temperature. When the blending amount of SCCB was 5%, the melting rate of the solid phase was the lowest. When the temperature reached 1400 °C, 21.32% of the solid phase remained unmelted. As the SCCB blending amount increased, the content of albite ($NaAlSi_3O_8$) first increased and then decreased. When the blending amount was 10%, the albite content ($NaAlSi_3O_8$) was the highest. The content of high-melting anorthite ($CaAl_2Si_2O_8$) in the ash did not change significantly, which is consistent with the slight change in the CaO content in the ash. After the SCCB blending amount was increased to 15%, new calcium aluminate (Ca (Al, Fe)$_{12}O_{19}$) and

nepheline ($NaAlSiO_4$) crystal phases formed in the slag, and the melting point was less than 1356 °C, which did not affect the changing trend of the liquidus temperature. At this time, the high-melting-point quartz (SiO_2) crystal phase disappeared. When the SCCB blending amount reached 25%, Na_2O reacted with Al_2O_3 and SiO_2 to generate a significant amount of nepheline ($NaAlSiO_4$). At this time, the crystalline phase was comprised primarily of nepheline ($NaAlSiO_4$) and calcium aluminate (Ca (Al, Fe)$_{12}O_{19}$), which increased the ash melting temperature of SCCB-25.

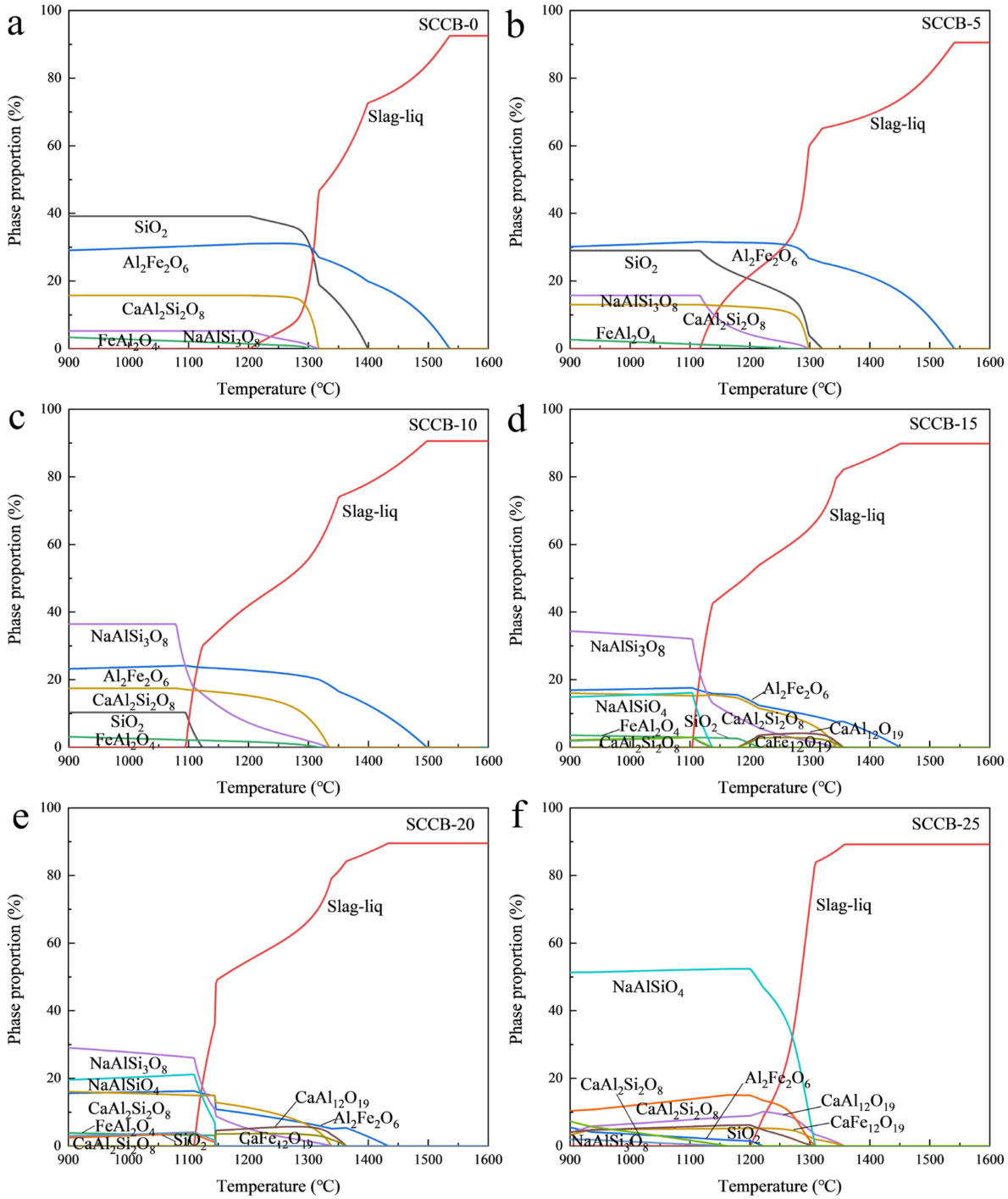


Figure 6. Mineral evolution maps of ash mixtures of meager coal and SCCB. (**a**) SCCB-0, (**b**) SCCB-5, (**c**) SCCB-10, (**d**) SCCB-15, (**e**) SCCB-20, (**f**) SCCB-25.

The analysis above indicates that the following reactions may occur during the co-combustion of meager coal and SCCBs at different proportions:

$$Fe_2O_3(s)+Al_2O_3(s) \rightarrow Al_2O_3 \cdot Fe_2O_3(s) \quad (1)$$

$$CaO(s)+Al_2O_3(s)+2SiO_2(s) \rightarrow CaAl_2Si_2O_8(s) \quad (2)$$

$$Na_2O(s)+Al_2O_3(s)+6SiO_2(s) \rightarrow 2NaAlSi_3O_8(s) \quad (3)$$

$$CaO(s)+6Fe_2O_3(s)+6Al_2O_3(s) \rightarrow Ca(Al,Fe)_{12}O_{19}(s)+9O_2(g) \quad (4)$$

$$Na_2O(s)+Al_2O_3(s)+2SiO_2(s) \rightarrow 2NaAlSiO_4(s) \quad (5)$$

3.5. Mineral Analysis of Ash

The XRD characterization of the ash from the co-combustion samples of meager coal and SCCBs after a complete combustion at 815 °C is shown in Figure 7. SiO_2 (2θ = 26.61°, 35.21°, 60.08°, and 68.11°) is the dominant substance in the co-combustion ash, which is consistent with the results of XRF. $CaSO_4$ is observed at 2θ = 25.54°, which is obtained by the further oxidation of $CaSO_3$ generated by the reaction of CaO with SO_2 released by coal combustion. In addition, Al_2O_3 (2θ = 20.71° and 22.98°), $CaAl_2Si_2O_8$ (2θ = 20.85° and 50.13°), and $Ca_3Al_2O_6$ (2θ = 35.20°) are observed. Al_2O_3 belongs to bridge oxide, which plays a link role to the substances in the ash. With the increase of mixing amount, the content of $NaAlSiO_4$ (2θ = 7.70°) in combustion ash increases and reaches the highest value when the mixing amount is 15%. This means that an increase in sodium content can accelerate the formation of low melting sodium-bearing minerals.

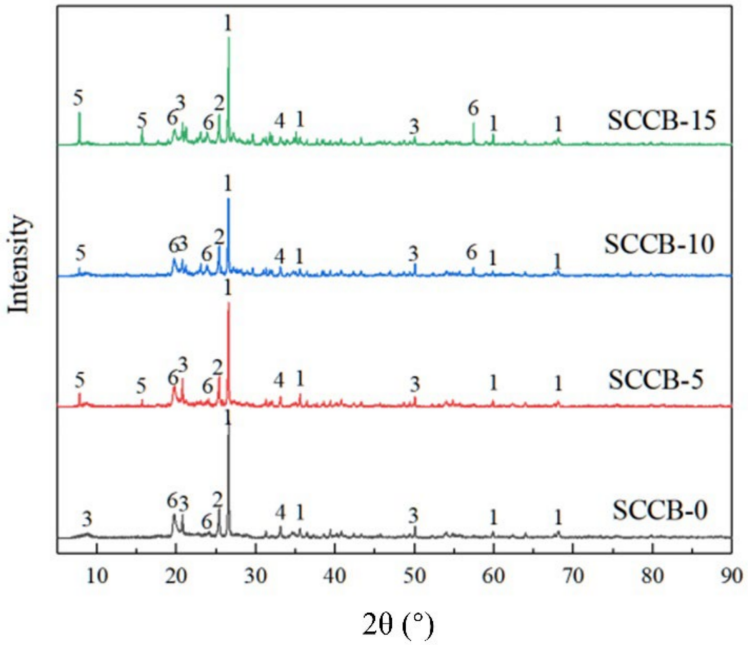


Figure 7. XRD results of co-combustion ash of SCCB-X (1-SiO_2, 2-$CaSO_4$, 3-$CaAl_2Si_2O_8$, 4-$Ca_3Al_2O_6$, 5-$NaAlSiO_4$, and 6-Al_2O_3).

3.6. Analysis of Viscous Temperature Characteristics of Ash

Figure 8 shows that as the amount of SCCB blending increased, the viscosity first decreased and then increased, and the viscosity of the ash residue of SCCB-5 was the lowest under the same temperature condition. Figure 9 shows the critical viscosity temperature (t_{cv}) and the lowest operating temperature (t_{lp}) of SCCB-X. Under the condition of SCCB-5, the sample ash slag indicated the lowest t_{cv} and t_{lp}, are 1368 °C and 1395 °C, respectively, lower than the flow temperature of coal ash (FT greater than 1400 °C). Thus, the heating surface of the boiler will not form a serious fusion.

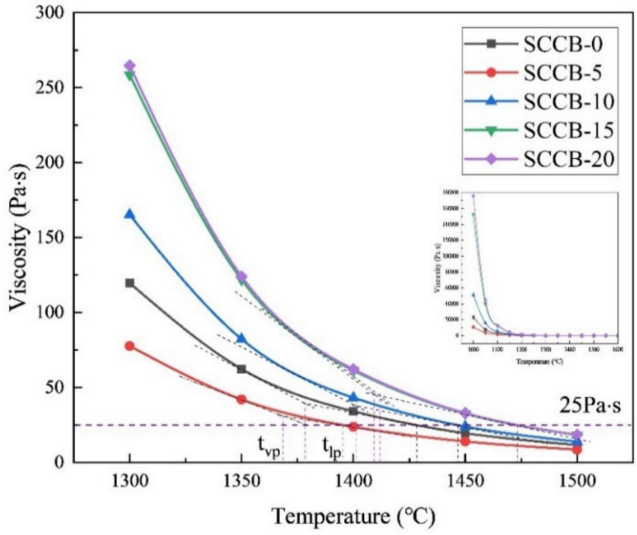


Figure 8. Viscosity curves of ash mixtures of meager coal and SCCB.

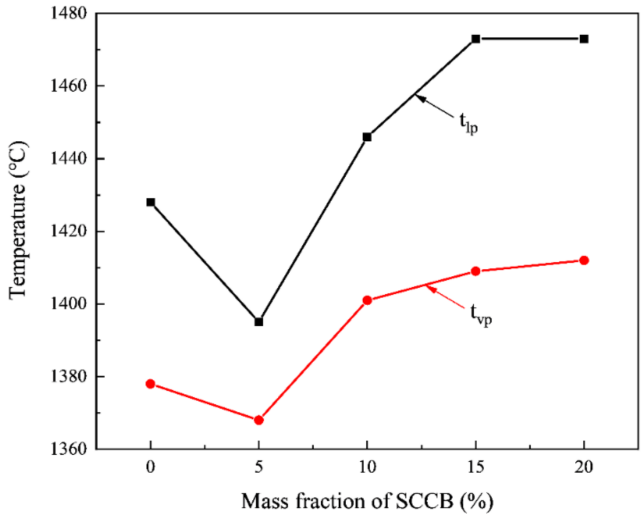


Figure 9. Effect of SCCB content on critical viscosity temperature and minimum operating temperature of ash.

The ash viscosity was determined based on both the solid-phase and liquid-phase composition [50]. As the blending amount of the SCCBs increased, the SiO_2 content decreased, and the viscosity of the ash melt decreased. By contrast, when the content of Al_2O_3 increased beyond 24%, the melt viscosity increased with the Al_2O_3 content. When the decrease in viscosity caused by the decrease in SiO_2 was smaller than the increase in viscosity caused by the increase in Al_2O_3, the overall viscosity of the ash slag increased. In addition, the decrease in MgO contributed to the increase in the viscosity of the ash slag.

3.7. Analysis of Ash Surface Morphology

Figure 10 shows the microscopic morphology of the burnt ash. Figure 10a shows that when the combustion temperature is 815 °C, the coal ash is partially melted and presents an agglomeration granular structure with a large number of broken particles attached to the surface. The results of EDS analysis indicate that the main components of coal ash are SiO_2 and Al_2O_3. As shown in Figure 10b, when adding 5 wt.% SCCB, the agglomerated ash particles decrease in diameter and increase in quantity, the sheet structure attached to the surface reduces, and the melting phenomenon is slightly relieved. Figure 10c figures that when the mixing ratio of SCCB rises to 10%, the ash surface is coated with flake particles and the agglomeration phenomenon is aggravated. As shown in Figure 10d, when the

mixing ratio of SCCB increases to 15%, the ash surface is coated with multilayer flake particles, and the agglomeration phenomenon is further deepened. The results of EDS analysis show that with the increase of the mixing ratio of SCCBs, the sodium content increases, while the silicon and aluminum content are low, which is consistent with the results of XPS. Because the combustion temperature is only 815 °C, no obvious melting and coking phenomenon is observed in the ash of the four samples.

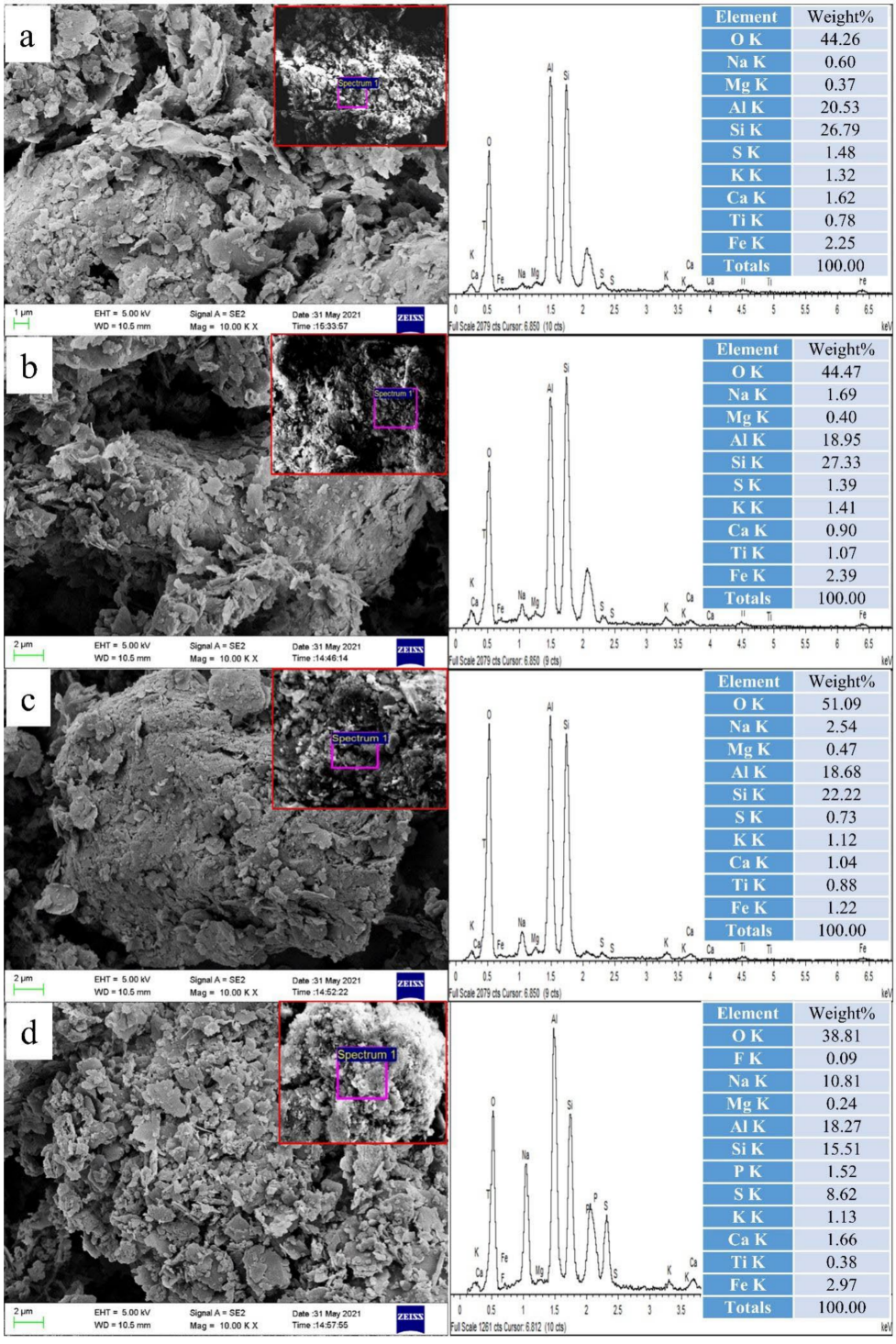


Figure 10. SEM images of burnt ash of SCCB-X samples. (**a**) SCCB-0, (**b**) SCCB-5, (**c**) SCCB-10, (**d**) SCCB-15.

3.8. Influence of Additive on the Co-Combustion Ash of SCCB-5

3.8.1. Effect of Additive on Mineral Composition

As shown in Figure 11, when the mixing ratio of CaO reaches 5%, the mineral phase in the slag changes greatly with temperature. The contents of composite oxides ($Al_2O_3 \cdot Fe_2O_3$), albite ($NaAlSi_3O_8$), and quartz (SiO_2) decrease, the content of anorthite ($CaAl_2Si_2O_8$) and mullite ($3Al_2O_3 \cdot 2SiO_2$) increase. The temperature of the appearing liquid phase of ash slag increases from 1118 °C to 1190 °C, and the liquidus temperature increases from 1540 °C to 1590 °C. This is because the increase of CaO promotes the formation of anorthite [51], whose melting point is 1550 °C, and inhibits the destruction of the polymers in the ash by Na, which makes the main solid phase in the ash mainly mullite and anorthite, leading to the increase of liquidus temperature. This also means that adding CaO can improve the ash melting characteristics.

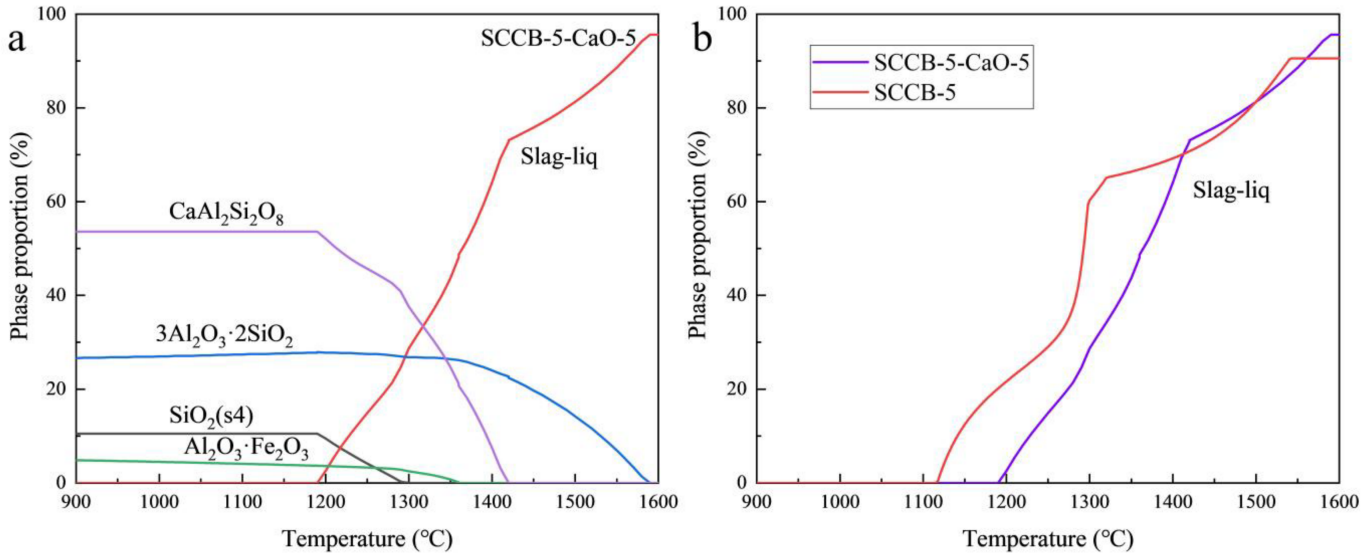


Figure 11. Influence of CaO on the mineral composition of co-combustion ash. (**a**) mineral evolution maps of ash of SCCB-5-CaO-5, (**b**) Liquidus curve.

3.8.2. Effect of Additive on Viscosity Characteristics of Ash

As shown in Figure 12, when the mixing ratio of CaO reaches 5%, the viscosity of SCCB-5 ash increases, t_{cv} and t_{lp} increases to 1418 °C and 1436 °C, respectively. The increase of CaO content leads to the decrease of Al_2O_3 and SiO_2 content. However, when the decrease in viscosity caused by the increase in CaO content is smaller than that caused by the increase of Al_2O_3 and SiO_2 content, the viscosity of slag will increase on the whole, which also indicates that adding a small amount of CaO will not improve the viscosity of the slag.

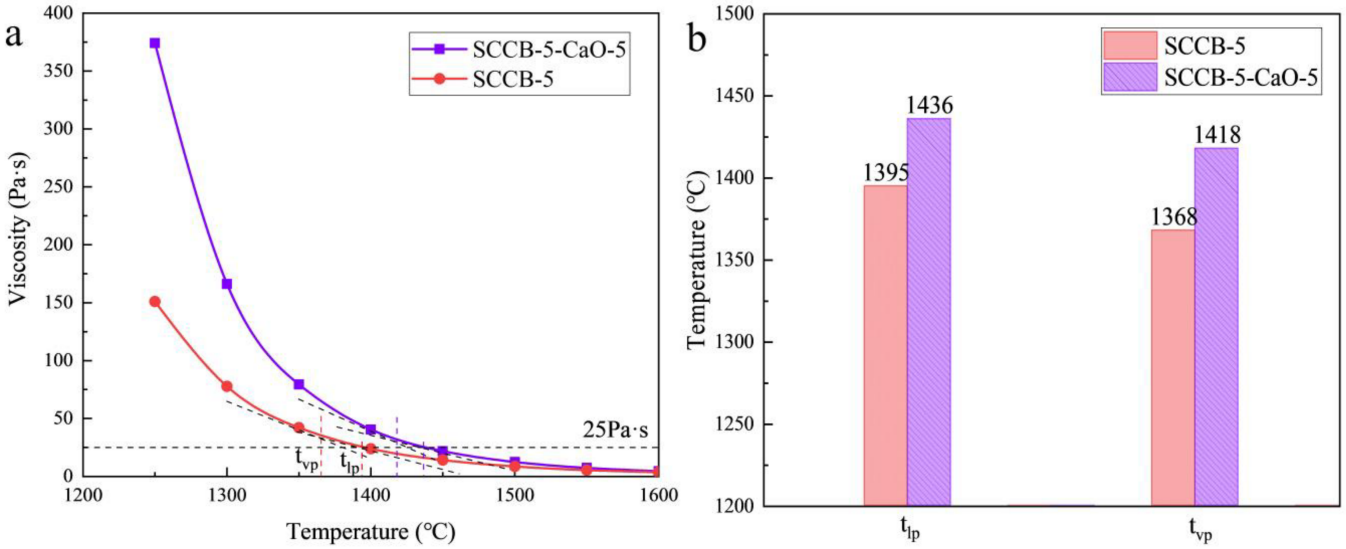


Figure 12. Influence of CaO on viscosity-temperature characteristics of co-combustion ash. (**a**) viscosity, (**b**) temperature.

4. Conclusions

In this study, the effect of different proportions of meager coal and SCCB co-combustion on ash fusion performance was investigated. It is found that the ash melting characteristics can be improved by mixing the proper proportion of SCCB in meager coal. When the mixing amount of SCCB is 5%, the slag viscosity index and slagging index are 83.83 and 1383 °C, respectively. In this condition, the co-combustion ash exhibits the lowest slagging tendency, and the ash particles produced by the co-combustion of meager coal and SCCB are fine and dispersed. In this case, the critical viscosity temperature and the minimum operating temperature of the ash residue are at 1368 °C, and 1395 °C, respectively, which are also the lowest, and the slag removal effect is better. If the mixing amount continues to increase, the tendency of cinder coking will increase, which is not conducive to slag discharge. Adding a suitable and small amount of CaO to SCCB-5 can improve the ash melting characteristics of co-combustion ash.

Supplementary Materials: The following supporting information can be downloaded at: https://www.mdpi.com/article/10.3390/en16020736/s1, Table S1 The characteristic temperature of ash after co-combustion of mixed sample.

Author Contributions: J.Z.: Conceptualization, Methodology, Formal analysis, Writing-original draft, Writing—review & editing, Visualization. Z.L.: Writing—review & editing. X.L.: Investigation. B.W.: Writing-review. Z.T.: Formal analysis. K.H.: Methodology, Supervision, Project administration, Funding acquisition. All authors have read and agreed to the published version of the manuscript.

Funding: This work was financially supported by Shandong Weiqiao Aluminum Power Co., Ltd (1380020011).

Data Availability Statement: No data was used for the research described in the article.

Conflicts of Interest: The authors declare that they have no known competing financial interests or personal relationships that could have appeared to influence the work reported in this paper.

References

1. Zhao, H.L.; Liu, F.Q.; Xie, M.Z.; Liu, W.; Sohn, H.Y. Recycling and utilization of spent potlining by different high temperature treatments. *J. Clean. Prod.* **2021**, *289*, 125704. [CrossRef]
2. Xiao, J.; Zhang, L.Y.; Yuan, J.; Yao, Z.; Tang, L.; Wang, Z.; Zhang, Z. Co-utilization of spent pot lining and coal gangue by hydrothermal acid-leaching method to prepare silicon carbide powder. *J. Clean. Prod.* **2018**, *204*, 848–860. [CrossRef]
3. Silveira, B.I.; Dantas, A.E.; Blasquez, J.; Samtos, R.K.P. Characterization of inorganic fraction of spent potliners: Evaluation of the cyanides and fluorides content. *J. Hazard. Mater.* **2002**, *89*, 177–183. [CrossRef] [PubMed]

4. Palmieri, M.J.; Andrade, L.F.; Trento, M.V.C.; Eleuterio, M.W.D.; Luber, J.; Davide, L.C.; Marcuss, S. Cytogenotoxic effects of spent pot liner (SPL) and its main components on human leukocytes and meristematic cells of Allium cepa. *Water Air Soil Pollution.* **2016**, *227*, 156. [CrossRef]
5. Shi, Z.N.; Li, W.; Hu, X.W.; Ren, B.J.; Gao, B.L.; Wang, Z.W. Recovery of carbon and cryolite from spent pot lining of aluminium reduction cells by chemical leaching. *Trans. Nonferrous Met. Soc. China* **2012**, *22*, 222–227. [CrossRef]
6. Xie, M.Z.; Li, R.B.; Zhao, H.L.; Liu, W.; Lu, T.T.; Liu, F.Q. Detoxification of spent cathode carbon blocks from aluminum smelters by joint controlling temperature-vacuum process. *J. Clean. Prod.* **2020**, *249*, 119370. [CrossRef]
7. Xiao, J.; Yuan, J.; Tian, Z.L.; Yang, K.; Yao, Z.; Yu, B.L.; Zhang, L.Y. Comparison of ultrasound-assisted and traditional caustic leaching of spent cathode carbon (SCC) from aluminum electrolysis. *Ultrason. Sonochemistry* **2018**, *40*, 21–29. [CrossRef]
8. Li, N.; Xie, G.; Wang, Z.X.; Hou, Y.Q.; Li, R.X. Recycle of spent potlining with low carbon grade by floatation. In *Chemical, Material and Metallurgical Engineering*, 3rd ed.; Trans Tech Publications Ltd.: Bäch, Switzerland, 2014. [CrossRef]
9. Wang, Y.F.; Chen, X.P. Discussion on recycling of spent cathode carbon blocks from aluminum smelters. *Light Met.* **2020**, *5*, 31–35. [CrossRef]
10. Renó, M.L.G.; Torres, F.M.; Silva, R.J.; Santos, J.J.C.S.; Melo, M.D.N.M. Exergy analyses in cement production applying waste fuel and mineralizer. *Energy Convers. Manag.* **2013**, *75*, 98–104. [CrossRef]
11. Zhao, H.L.; Ma, B.Z.; Hong, S.; Huang, H.; Liu, F.Q.; Sohn, H.Y. Recovery of Copper and Cobalt from Converter Slags via Reduction–Sulfurization Smelting Using Spent Pot Lining as the Reductant. *ACS Sustain. Chem. Eng.* **2021**, *9*, 4234–4246. [CrossRef]
12. Thomanetz, E. Solid recovered fuels in the cement industry with special respect to hazardous waste. *Waste Manag. Res.* **2012**, *30*, 404–412. [CrossRef]
13. Jiang, X.G.; Li, Y.H.; Yan, J. Hazardous waste incineration in a rotary kiln: A review. *Waste Dispos. Sustain. Energy.* **2019**, *1*, 3–37. [CrossRef]
14. Zhang, S.R.; Jiang, X.G.; Lv, G.J.; Liu, B.X.; Jin, Y.Q.; Yan, J.H. SO_2, NOx, HF, HCl and PCDD/Fs emissions during Co-combustion of bituminous coal and pickling sludge in a drop tube furnace. *Fuel* **2016**, *186*, 91–99. [CrossRef]
15. Han, D.; Jiang, X.G.; Lv, G.J.; Yong, C.; Yan, J.H. Co-combustion of tannery sludge in a commercial circulating fluidized bed boiler. *Waste Manag.* **2015**, *46*, 227–233. [CrossRef]
16. Zhang, J.; Teng, Z.C.; Han, K.H.; Li, Y.J.; Wang, M.M. Co-combustion characteristics and kinetics of meager coal and spent cathode carbon block by TG-MS analysis. *Arab. J. Chem.* **2021**, *14*, 103198. [CrossRef]
17. Dai, H.L.; Shi, S.W.; Yang, L.; Guo, C.; Chen, X. Recent progress on the corrosion behavior of metallic materials in HF solution. *Corros. Res.* **2021**, *39*, 313–337. [CrossRef]
18. Li, X.M.; Zhi, L.F.; Shi, W.J.; Kong, L.X.; Bai, J.; Yu, J.L.; Reinmoller, M.; Guhl, S.; Meyer, B.; Li, W. Effect of K_2O/Na_2O on fusion behavior of coal ash with high silicon and aluminum level. *Fuel* **2020**, *265*, 116964. [CrossRef]
19. Vassilev, S.V.; Kitano, K.; Takedab, S.; Tsurue, T. Influence of mineral and chemical composition of coal ashes on their fusibility. *Fuel Process. Technol.* **1995**, *45*, 27–51. [CrossRef]
20. Oleschko, H.; Muller, M. Influence of coal composition and operating conditions on the release of alkali species during combustion of hard coal. *EnergyFuels* **2007**, *21*, 3240–3248. [CrossRef]
21. Van Dyk, J.; Waanders, F.B.; Benson, S.A.; Laumb, M.L.; Hack, K. Viscosity predictions of the slag composition of gasified coal, utilizing FactSage equilibrium modelling. *Fuel* **2009**, *88*, 67–74. [CrossRef]
22. Su, S.; Pohl, J.H.; Holcombe, D.; Hart, J.A. Techniques to determine ignition, flame stability and burnout of blended coals in p.f. power station boilers. *Prog. Energy Combust. Sci.* **2001**, *27*, 75–98. [CrossRef]
23. Su, S.; Pohl, J.; Holcombe, D.; Hart, J.A. Slagging propensities of blended coals. *Fuel* **2001**, *80*, 1351–1360. [CrossRef]
24. Qiu, J.R.; Li, F.; Zheng, Y.; Zheng, C.G.; Zhou, H.C. The influences of mineral behaviour on blended coal ash fusion characteristics. *Fuel* **1999**, *78*, 963–969. [CrossRef]
25. Wall, T.F.; Creelman, R.A.; Gupta, R.P.; Gupta, S.K.; Coin, C.; Lowe, A. Coal ash fusion temperatures-New characterization techniques, and implications for slagging and fouling. *Prog. Energy Combust. Sci.* **1998**, *24*, 345–353. [CrossRef]
26. Bryers, R.W. Fireside slagging, fouling, and high-temperature corrosion of heat-transfer surface due to impurities in steam-raising fuels. *Prog. Energy Combust. Science.* **1996**, *22*, 29–120. [CrossRef]
27. Degereji, M.U.; Ingham, D.B.; Ma, L.; Pourkashanian, M.; Williams, A. Prediction of ash slagging propensity in a pulverized coal combustion furnace. *Fuel* **2012**, *101*, 171–178. [CrossRef]
28. Huang, L.Y.; Norman, J.; Pourkashanian, M.; Williams, A. Prediction of ash deposition on superheater tubes from pulverized coal combustion. *Fuel* **1996**, *75*, 271–279. [CrossRef]
29. Adell, V.; Cheeseman, C.R.; Ferraris, M.; Salvo, M.; Smeacetto, F.; Boccaccini, A.R. Characterising the sintering behaviour of pulverised fuel ash using heating stage microscopy. *Mater. Charact.* **2007**, *58*, 980–988. [CrossRef]
30. Wang, L.; Skjevrak, G.; Hustad, J.; Grønli, M. Sintering characteristics of sewage sludge ashes at elevated temperatures. *Fuel Process. Technol.* **2012**, *96*, 88–97. [CrossRef]
31. Chen, Z.H.; Liu, J.; Chen, L.G.; Evrendilek, F.; Xie, W.M.; Wu, X.Y.; Hu, J.W.; Li, W.X. Emission-to-ash detoxification mechanisms of co-combustion of spent pot lining and pulverized coal. *J. Hazard. Mater.* **2021**, *418*, 126380. [CrossRef]
32. Wang, Y.; Xiang, Y.; Wang, D.X.; Dong, C.Q.; Yang, Y.P.; Xiao, X.B.; Lu, Q.; Zhao, Y. Effect of sodium oxides in ash composition on ash fusibility. *Energy Fuels* **2016**, *30*, 1437–1444. [CrossRef]

33. Dai, X.; Bai, J.; Huang, Q.; Liu, Z.; Bai, X.J.; Cao, R.G.; Wen, X.D.; Li, W.; Du, S.Y. Viscosity temperature properties from molecular dynamics simulation: The role of calcium oxide, sodium oxide and ferrous oxide. *Fuel* **2019**, *237*, 163–169. [CrossRef]
34. Zhu, Y.M.; Tan, H.Z.; Niu, Y.Q.; Wang, X.B. Experimental study on ash fusion characteristics and slagging potential using simulated biomass ashes. *J. Energy Inst.* **2019**, *92*, 1889–1896. [CrossRef]
35. Ma, X.W.; Li, F.H.; Ma, M.J.; Fang, Y.T. Investigation on blended ash fusibility characteristics of biomass and coal with high silica-alumina. *Energy Fuels* **2017**, *31*, 7941–87951. [CrossRef]
36. Shi, W.J.; Kong, L.X.; Bai, J.; Xu, J.; Li, W.C.; Bai, Z.Q.; Li, W. Effect of CaO/Fe_2O_3 on fusion behaviors of coal ash at high temperatures. *Fuel Process. Technol.* **2018**, *181*, 18–24. [CrossRef]
37. Vargas, S.; Frandsen, F.; Dam-Johansen, K. Rheological properties of high-temperature melts of coal ashes and other silicates. *Prog. Energy Combust. Sci.* **2001**, *27*, 237–429. [CrossRef]
38. Zhao, Y.L.; Zhang, Y.M.; Bao, S.X.; Chen, T.J.; Liu, X. Effect of stone coal chemical composition on sintering behavior during roasting. *Ind. Eng. Chem. Res.* **2014**, *53*, 157–163. [CrossRef]
39. Yao, X.Y. Relationship of coal ash fusibility to chemical composition. *J. Fuel Chem. Technol.* **1965**, *6*, 151–161.
40. Wang, Y.; Wang, D.X.; Dong, C.Q.; Yang, Y.P. The behavior and reactions of sodium containing minerals in ash melting process. *J. Energy Inst.* **2017**, *90*, 167–173. [CrossRef]
41. Zheng, Y.J.; Jensen, P.A.; Jensen, A.D. A kinetic study of gaseous potassium capture by coal minerals in a high temperature fixed-bed reactor. *Fuel* **2008**, *87*, 3304–3312. [CrossRef]
42. Clery, D.S.; Mason, P.E.; Rayner, C.M.; Jones, J.M. The effects of an additive on the release of potassium in biomass combustion. *Fuel* **2018**, *214*, 647–655. [CrossRef]
43. Mu, L.; Zhao, C.; Zhao, L.; Chen, B.W.; Xu, Z.L.; Yang, Z.Q.; Shang, Y.; Yin, H.C. Mineralogical composition evolution and thermogravimetric characteristics of sewage sludge ash at different ashing temperatures. *Energy Fuels* **2018**, *32*, 12617–12629. [CrossRef]
44. Liu, S.Q.; Qi, C.; Jiang, Z.; Zhang, Y.J.; Niu, M.F.; Li, Y.Y.; Dai, S.F.; Finkelman, R.B. Mineralogy and geochemistry of ash and slag from coal gasification in China: A review. *Int. Geol. Rev.* **2018**, *60*, 717–735. [CrossRef]
45. Xie, L.C.; Xu, L.; Ma, X.X. Influence of the direct coal liquefaction residue on the fusion characteristics of Jincheng coal with a high ash fusion temperature. *Energy Fuels* **2020**, *34*, 1355–1364. [CrossRef]
46. Li, F.H.; Li, M.; Fan, H.L.; Fan, Y.T. Understanding Ash Fusion and Viscosity Variation from Coal Blending Based on Mineral Interaction. *Energy Fuels* **2018**, *32*, 142–151. [CrossRef]
47. Zhou, Y.G.; Fan, J.; Li, P.; Wang, B.H.; Zhao, H. Mineral transmutation of high alkali Zhundong coal in ash melting process. *J. Zhejiang Univ.* **2015**, *49*, 1559–1564. [CrossRef]
48. Labbafan, A.; Ghassemi, H. Numerical modeling of an E-Gas entrained flow gasifier to characterize a high-ash coal gasification. *Energy Convers. Manag.* **2016**, *112*, 337–349. [CrossRef]
49. Ren, H.J.; Zhang, Y.Q.; Fang, Y.T. Co-gasification behavior of meat and bone meal char and coal char. *Fuel Process. Technol.* **2011**, *92*, 298–307. [CrossRef]
50. Ji, H.S.; Li, Z.Q.; Zhou, Y.; Qi, Y.; He, Z.X. The research on viscosity-temperature characteristics of the mixed slag of biomass and bituminous coal. *J. Fuel Chem. Technol.* **2021**, *49*, 11–19. [CrossRef]
51. Zhang, C.X.; Li, Y.J.; He, Z.R.; Zhao, J.L.; Wang, D. Microtubular Fe/Mn-promoted $CaO\text{-}Ca_{12}Al_{14}O_{33}$ bifunctional material for H_2 production from sorption enhanced water gas shift. *Appl. Catal. B Environ.* **2022**, *314*, 121474. [CrossRef]

Disclaimer/Publisher's Note: The statements, opinions and data contained in all publications are solely those of the individual author(s) and contributor(s) and not of MDPI and/or the editor(s). MDPI and/or the editor(s) disclaim responsibility for any injury to people or property resulting from any ideas, methods, instructions or products referred to in the content.